



Kinetic model for the reversible deactivation of a Pt/Al₂O₃ catalyst during NO oxidation

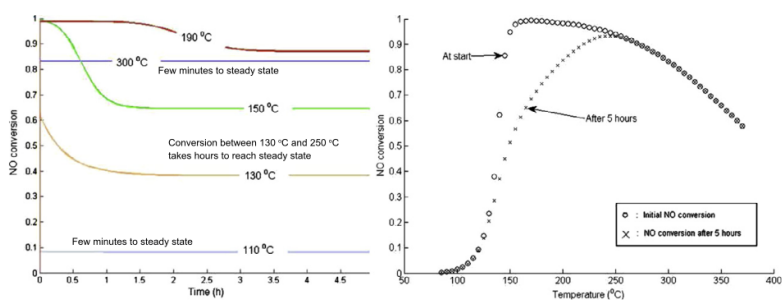
Rushap Khazanchi, Divakar Reddy, Divesh Bhatia *

Department of Chemical Engineering, Indian Institute of Technology Delhi, Hauz Khas, New Delhi 110016, India

HIGHLIGHTS

- Global kinetic model is developed for reversible deactivation of Pt/Al₂O₃ catalyst during NO oxidation.
- Inverse hysteresis phenomenon is predicted by the model.
- Steady state is achieved in a few minutes at high and low temperatures and in a few hours at intermediate temperatures.
- Regain of catalyst activity in N₂ is due to enhanced decomposition of Pt oxides at high temperatures.

GRAPHICAL ABSTRACT



ARTICLE INFO

Article history:

Received 14 September 2016

Received in revised form 8 December 2016

Accepted 10 December 2016

Available online 16 December 2016

Keywords:

Inverse hysteresis
NO oxidation
Reversible deactivation
Pt oxides
Global kinetics
Pt/Al₂O₃

ABSTRACT

Microkinetic approach is used to develop a kinetic model for the reversible deactivation of a Pt/Al₂O₃ catalyst during NO oxidation. The model predicts the dependence of temperature on the transient evolution of NO conversion. Consistent with literature, it is shown that for low and high temperatures, it takes a few minutes to achieve steady state, whereas for intermediate temperatures (>130 °C and <250 °C), the time taken is of the order of a few hours. The model explains the inverse hysteresis phenomenon reported in the literature. In contrast to other works, the effect of NO₂ as well as O₂ on the catalyst deactivation is considered. The restoration of catalyst activity is explained by the reduction of Pt oxides by NO at low temperatures and the thermal decomposition of Pt oxides at high temperatures. The effect of inlet NO concentration, gas hourly space velocity, and temperature ramp rates on the light-off behavior is captured accurately by the model. The effect of gas composition during cooling, maximum temperature during heating, minimum temperature during cooling, and catalyst exposure to various gases at a fixed temperature on the NO oxidation activity in the subsequent runs is predicted. Consistent with the literature, the model predicts that cooling in the presence of N₂ only can result in a significant restoration of the catalyst activity, provided that the catalyst has been exposed to high temperatures (>300 °C) before the start of cooling. This has been attributed to the enhanced decomposition of Pt oxides at high temperatures. It is also shown that exposing the catalyst to NO at low temperatures for long time periods can result in a regain of the catalyst activity.

© 2016 Elsevier B.V. All rights reserved.

1. Introduction

With the increasing number of vehicles on the roads, the emission norms are becoming stringent by the day. Automobile

manufacturers and catalyst companies all around the globe have been coming up with newer and better technologies to keep pace with the increasingly stringent norms. Such technologies have significantly brought down the concentrations of NO_x that are emitted from the engine. Diesel oxidation catalysts are widely employed as the first catalysts in both NSR and SCR diesel NO_x control systems. Besides oxidation of CO and unburnt hydrocarbons,

* Corresponding author.

E-mail address: dbhatia@chemical.iitd.ac.in (D. Bhatia).

Nomenclature

<i>a</i>	side length of square channel (m)	\bar{u}	average gas velocity in the channel (m/s)
A_{bi}	reverse rate pre-exponential factor for microkinetic step Ri (mol/m ³ washcoat-s)	$X_{j,wc}$	dimensionless concentration of species <i>j</i> at fluid-washcoat interface
A_{fi}	forward rate pre-exponential factor for microkinetic step Ri (mol/m ³ washcoat-s)	X_{jm}	dimensionless cup-mixing concentration of species <i>j</i> in axial position (m)
C_T	total Pt sites (mol/m ³ washcoat)	ΔG	Gibbs free energy change for the reaction (kJ/mol)
C_{Pt_Active}	total active Pt sites (mol/m ³ washcoat)	$\Delta G^{kin,6}$	Gibbs free energy change for reaction (R8) obtained by using the kinetic parameters of reactions (R2), (R5) and (R7) (kJ/mol)
$C_{Pt_Inactive}$	total inactive Pt sites (mol/m ³ washcoat)	$\Delta G^{kin,7}$	Gibbs free energy change for reaction (R8) obtained by using the kinetic parameters of reactions (R1)–(R3), (R5) and (R6) (kJ/mol)
c_{Tm}	total molar concentration (mol/m ³)	ΔG_{PtO}^{thermo}	Gibbs free energy change of PtO formation (kJ/mol)
C_v	concentration of vacant active Pt sites (mol/m ³ washcoat)	$\Delta G_{PtO_2}^{thermo}$	Gibbs free energy change of PtO ₂ formation (kJ/mol)
D_{mj}	diffusivity of specie <i>j</i> in gas phase (m ² /s)	ΔH	enthalpy change of a reaction obtained by a linear combination of the various microkinetic reactions (kJ/mol)
E_{bi}	reverse activation energy of step Ri (kJ/mol)	ΔH_i	enthalpy change of an <i>i</i> th reaction in a microkinetic reaction mechanism (kJ/mol)
E_{fi}	forward activation energy of step Ri (kJ/mol)	ΔS	entropy change of a reaction obtained by a linear combination of the various microkinetic reactions (kJ/mol-K)
k_{bi}	reverse rate constant for step Ri (mol/m ³ washcoat-s)	ΔS_i	entropy change of an <i>i</i> th reaction in a microkinetic reaction mechanism (kJ/mol-K)
k_{cj}	external mass transfer coefficient of specie <i>j</i> (m/s)	δ_c	washcoat thickness (m)
k_{fi}	forward rate constant for step Ri (mol/m ³ washcoat-s)	ε_{wc}	porosity of the washcoat
K_i	equilibrium constant for microkinetic step Ri	v_i	multiplicative factor for reaction <i>i</i>
PtO _x	deactivated Pt sites	ϑ_{ij}	stoichiometric coefficient of specie <i>j</i> in reaction <i>i</i>
<i>r</i>	number of reactions used in the linear combination	θ_{Pt_active}	fraction of active Pt sites
r_g	total number of reactions	$\theta_{Pt_inactive}$	fraction of inactive Pt sites
R_Ω	effective transverse length scale (m)		
R	universal gas constant (kJ/mol-K)		
R_{PtO_x-1}	rate of reaction for step (R6) (mol/m ³ washcoat-s)		
R_{PtO_x-2}	rate of reaction for reaction (R7) (mol/m ³ washcoat-s)		
R_{yi}	rate of reaction <i>i</i> (mol/m ³ washcoat-s)		
Sh_Ω	Sherwood number		
T_s	temperature of the washcoat (K)		
<i>t</i>	time (s)		

formation of NO₂ by NO oxidation takes place in a DOC, which plays an important role in both NSR and SCR aftertreatment devices. This is because of the ease of NO₂ storage on alkaline earth metals of the NSR catalyst in comparison to NO storage [1]. Also, the oxidation of NO to NO₂ assists in achieving a NO:NO₂ ratio close to 1:1, which creates local fast SCR conditions and hence increases the rate of NO_x reduction reactions in the SCR.

Various groups have performed experiments on NO oxidation over Pt/Al₂O₃ and other platinum based catalysts under steady state conditions [1–7]. Transient variation of NO conversion during temperature ramps have also been reported [1,2,8]. An inhibitive effect of NO₂ on NO oxidation reaction was reported by several groups [4,5,7]. Mulla et al. [3] performed a kinetic study of the NO oxidation reaction over a Pt/Al₂O₃ catalyst and measured a near negative first order concentration dependence ($= -0.92$) with respect to NO₂.

Bhatia et al. [7] reported a continuous decrease in NO oxidation activity with time-on-stream and ascribed it to the deactivation caused by NO₂, which is distinct from the prompt inhibition observed with NO₂ in the feed. Similar results were reported by Olsson and Fridell [8] and were explained by the formation of platinum oxides or strongly chemisorbed oxygen on the catalyst surface. Both the research groups found that the deactivation caused by NO₂ during NO oxidation is reversible. Bhatia et al. [7] found that the catalyst activity was regained by reduction of the catalyst with H₂, whereas Olsson and Fridell [8] found that when a gas consisting of NO and O₂ was passed over a catalyst previously exposed to NO₂, the activity increased with time. To study the transient deactivation and re-activation of the catalyst, Hauptmann et al. [9] performed NO oxidation experiments over a Pt/Al₂O₃ catalyst under conditions of increasing and decreasing temperature ramps. The experiments were performed by ramping up the temperature from 80 °C to 370 °C, followed by a temperature ramp-down,

which brought the temperature back to 80 °C. It was observed that for a given temperature, the NO_x conversion was lower during the second half of the experiment, i.e., when the temperature decreased with respect to time. Their data showed trends opposite to that observed in the case of multiple steady-states, and hence the phenomenon was referred to as ‘inverse hysteresis’. They hypothesized that the reversible oxidation of platinum surface by NO₂ and the reduction of Pt surface by NO results in the observed inverse hysteresis behavior. Recently, Li et al. [10] showed that the observed hysteresis is not a result of multiple steady states but a result of slow change in the activity of the catalyst.

The oxidation of Pt surface and formation of Pt oxides has been studied by several groups [8,11–14]. According to Hwang and Yeh [11], the formation of surface platinum oxides starts around 25 °C with PtO becoming apparent at 100 °C and PtO₂ at 300 °C. As the temperature is increased further, platinum starts to react with Al₂O₃ forming PtAl₂O₄. The thermal decomposition of PtO_x at high temperatures was shown by XPS data reported by Peuckert and Bonzel [12]. Hauff et al. [13] showed that the type of oxides formed depends not only on the temperature but also on the type of support. Equivalent amount of Pt/Al₂O₃ was seen to have a lower O₂ uptake in comparison to other alumina and silica based automotive catalysts. Hauff et al. [13] explained this observation by a layer of surface oxides formed on the catalyst which restricts bulk diffusion of gases. McCabe et al. [14] studied the oxidation of Pt by gaseous oxygen for a series of silica and alumina supported Pt catalysts and reported that Platinum oxidation was limited to the surface layer of Pt atoms.

Kinetic models have been developed to explain the inverse hysteresis phenomenon [9,15]. Hauptmann et al. [9] extended their microkinetic model of NO oxidation to include the reversible deactivation of Pt active sites by 2 reactions: formation of oxidized Pt by NO₂ adsorbed on the active Pt sites and the reduction of

deactivated Pt sites by NO to release NO₂. However, they did not account for the deactivation of the sites by O₂, which is present in the reactant mixture in a significant amount. Hauff et al. [13] reported that at high temperatures exceeding 300 °C, the oxidized form of Pt becomes unstable and decomposes to Pt. However, the decrease in the amount of Pt oxides is not considered in the model by Hauptmann et al. [9]. In contrast to the microkinetic model of Hauptmann et al. [9], Hauff et al. [15] proposed a macro-kinetic model, which considers the reversible formation of Pt oxide by O₂ and the irreversible reduction of PtO by NO. However, the formation of Pt oxides by NO₂ was not considered in the model. They argued that at low concentrations of NO₂ (<200 ppm), the effect of NO₂ on Pt oxide formation is negligible. However, the data used in the current work is taken from Hauptmann et al. [9], who did experiments with NO concentrations as high as 450 ppm NO, and could result in NO₂ concentrations of a similar magnitude. Also, it has been discussed by several researchers that NO₂ is a stronger oxidizing agent than O₂ [7,9]. Hence, the assumption of negligible effect of NO₂ on Pt oxides formation is not applicable for the present analysis.

In this work, a global kinetic model is developed using a microkinetics approach for the reversible deactivation of a Pt/Al₂O₃ catalyst during NO oxidation. The kinetic model for NO oxidation used in the present work is thermodynamically consistent and considers the inhibiting effect of NO₂. The formation of Pt oxides due to the presence of NO₂ and O₂ is considered, which explains the slow decrease in the catalyst activity. The variation of NO conversion with time for various temperatures is predicted by the model, and the dependence of temperature on the time taken to achieve steady state is explained. The gradual re-gain of catalyst activity, referred to as reactivation in the present work is explained by considering the reduction of Pt oxides by NO. Thermal decomposition of Pt oxides is incorporated in the model to explain the high-temperature instability of Pt oxides, reported by Hauff et al. [13]. The model is used to predict the inverse hysteresis phenomenon reported by Hauptmann et al. [9] and the modelling results are validated against their experimental data. Simulations are performed for various experimental protocols and the results are compared with the trends reported in the literature.

2. Model development

We start with a brief summary of the experiments, which form the basis for model development [9]. A monolithic diesel oxidation catalyst with a length of 7.6 cm, diameter of 2.54 cm and a cell density of 400 cpsi was used for the NO oxidation experiments performed by Hauptmann et al. [9]. The pressure range along the length of the monolith was 1.10–1.08 bar. NO and NO₂ concentrations at the end of the monolith were measured using a chemiluminescence detector. Pre-treatment was done using 3 vol% H₂ in N₂ at 370 °C with a subsequent cooling in N₂ atmosphere.

Various temperature programs were employed for the experimental runs. All these experiments, invariably, had the following conditions – a temperature ramp rate of 5 °C/min with an initial temperature of 80 °C and a gas hourly space velocity of 25,000 h⁻¹. One such experiment involved increasing the temperature from 80 °C to 370 °C at a ramp rate of 5 °C/min, followed by a temperature ramp-down, back to 80 °C at the same ramp rate. Fig. 1 shows the experimental data when the inlet gas contained 450 ppm NO, 6% O₂, and remaining N₂. It is observed that at any given temperature, the NO conversion during temperature ramp-up is higher than that during the temperature ramp-down. This phenomenon is referred to as inverse hysteresis by Hauptmann et al. [9]. In the present work, we develop a global kinetic model

obtained from a micro-kinetics approach to predict the catalyst deactivation and the inverse hysteresis behavior reported by Hauptmann et al. [9].

2.1. Reactor model

A one-dimensional two-phase model is used to capture the phenomenon of convection, external mass transfer and reactions in the catalytic monolith [16]. Following is a list of assumptions used for development of the model:

- (a) Isothermal conditions prevail throughout the reactor because the concentration of reactant gases are low enough to cause any significant temperature change,
- (b) no heat loss to the surroundings,
- (c) rate of reaction inside the washcoat is assumed to be slow in comparison to the rate of diffusion of gases in the washcoat, i.e., washcoat diffusional limitations are neglected. This allows for a constant concentration of a reactant/product gas in the transverse direction within the washcoat, and
- (d) all channels are assumed identical and the species balance equations are written for one channel only.

The species balance equations in the gas phase and solid phase for a species *j* are given by Eqs. (1) and (2), respectively [16]. Please refer to Appendix B for the variation of mass transfer and kinetic rates with respect to temperature, i.e., the relative magnitudes of the two terms on the right hand side of Eq. (2).

$$\frac{\partial X_{jm}}{\partial t} + \bar{u} \frac{\partial X_{jm}}{\partial x} = -\frac{k_{cj}}{R_\Omega} (X_{jm} - X_{j,wc}) \quad (1)$$

$$\varepsilon_{wc} \frac{\partial X_{j,wc}}{\partial t} = \frac{k_{cj}}{\delta_c} (X_{jm} - X_{j,wc}) + \frac{\sum_{i=1}^{r_g} [\vartheta_{ij} R_{vi}(T_s, X_{wc})]}{c_{im}} \quad (2)$$

Here, k_{cj} is the mass transfer coefficient of species *j* and is obtained using

$$k_{cj} = \frac{Sh_\Omega D_{mj}}{R_\Omega} \quad (3)$$

Values of various physical parameters used in the reactor model are given in Table 1.

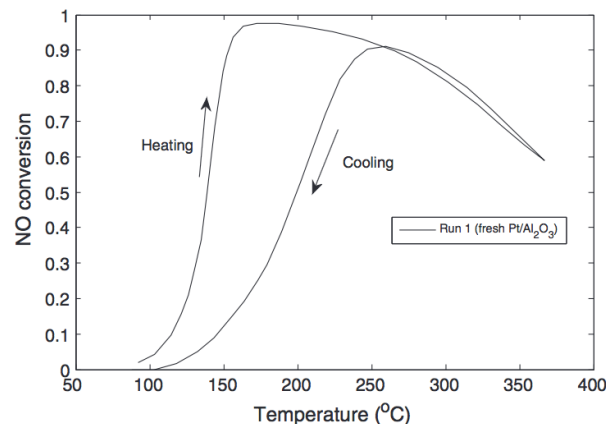


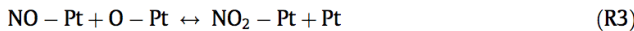
Fig. 1. Inverse hysteresis observed during NO oxidation on fresh Pt/Al₂O₃ catalyst [9].

2.2. Kinetic rate model

A global kinetic rate expression for NO oxidation was used as the first step in deriving our kinetic model and is given by Eq. (4) [7].

$$R_v = \frac{k_{f2}X_{O_2,wc} \left[1 - \frac{1}{X_{O_2,wc} K_2 K_5} \left(\frac{K_4 X_{NO_2,wc}}{K_1 K_3 X_{NO,wc}} \right)^2 \right]}{1 + K_1 X_{NO,wc} + \frac{K_4 X_{NO_2,wc}}{K_1 K_3 X_{NO,wc}}} \quad (4)$$

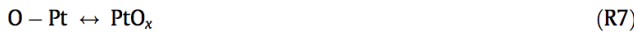
The rate expression was developed based on reactions (R1)–(R5) given below with (R2) assumed to be the rate limiting step [7].



The equilibrium constant for reaction R_i is represented by K_i and is given as

$$K_i = \frac{k_{fi}}{k_{bi}} = \frac{A_{fi} e^{-E_{fi}/RT_s}}{A_{bi} e^{-E_{bi}/RT_s}} \quad (5)$$

Eq. (4) does not consider the loss in activity of the catalyst with time. In order to predict the observed inverse hysteresis phenomenon during NO oxidation, we incorporated the deactivation of Pt into the model by assuming that Pt is present in two forms, namely active Pt in the metallic form and inactive Pt_{Ox}. It was reported that the inactive Pt could be in the form of PtO, PtO₂, strongly chemisorbed oxygen or PtAl₂O₄, with their relative proportions varying significantly with Pt dispersion and oxidation temperature [11,17]. McCabe et al. [14] also reported that they could not make a clear distinction between oxidic and chemisorbed oxygen. In the absence of further information on the form of inactive Pt, we do not speculate it and represent it by Pt_{Ox}. Further, the reactivation of Pt crystallites is accounted for by the following reversible reactions:



Forward reaction (R6) represents the formation of inactive Pt oxides by NO₂ whereas the reverse reaction (R6) represents the re-activation due to NO. Forward reaction (R7) represents the formation of inactive Pt oxides by chemisorbed oxygen whereas the reverse reaction (R7) represents the thermal decomposition of inactive Pt oxides back to the active form as chemisorbed oxygen, which typically takes place at high temperatures.

The global rate equation for NO oxidation (Eq. (4)) was multiplied by the fraction of active Pt sites ($\theta_{Pt,active}$) and the modified equation is given by Eq. (6). While developing the rate expression,

Table 1
Values of physical properties and other parameters used in the simulations.

Parameter	Numerical value
\bar{u}	0.546 m/s
L	0.076 m
δ_c	1.45×10^{-5} m
a	1.2×10^{-3} m
ε_{wc}	0.6
$D_{NO_2,m}$	3.42×10^{-5} m ² /s
$D_{NO,m}$	4.57×10^{-5} m ² /s
$D_{O_2,m}$	4.57×10^{-5} m ² /s
R_Ω	3×10^{-4} m
Sh_Ω	3.608

it was assumed that inactive platinum sites have zero activity towards NO oxidation.

$$R_v = \frac{\theta_{Pt,active} k_{f2} X_{O_2,wc} \left[1 - \frac{1}{X_{O_2,wc} K_2 K_5} \left(\frac{K_4 X_{NO_2,wc}}{K_1 K_3 X_{NO,wc}} \right)^2 \right]}{1 + K_1 X_{NO,wc} + \frac{K_4 X_{NO_2,wc}}{K_1 K_3 X_{NO,wc}}} \quad (6)$$

A balance over the total Pt sites resulted in Eq. (7), and is given as

$$\theta_{Pt,Active} + \theta_{Pt,Inactive} = 1 \quad (7)$$

Eq. (7) can be represented in terms of concentrations as

$$C_{Pt,Active} + C_{Pt,Inactive} = C_T \quad (8)$$

The rate of Pt oxides formation from adsorbed NO₂ and O₂, as per reactions (R6) and (R7), is represented by Eqs. (9) and (10), respectively.

$$R_{PtO_x-1} = k_{f6} C_{NO_2-Pt} - k_{b6} C_{Pt,Inactive} X_{NO,wc} \quad (9)$$

$$R_{PtO_x-2} = k_{f7} C_{O-Pt} - k_{b7} C_{Pt,Inactive} \quad (10)$$

The concentrations of adsorbed NO₂ and O were obtained by assuming that reactions (R1)–(R5), barring (R2), are in equilibrium and (R2) is the rate determining step for NO oxidation. The surface concentrations are represented in terms of gas-phase concentrations as

$$C_{O-Pt} = \frac{C_v K_4 X_{NO_2,wc}}{K_3 K_1 X_{NO,wc}} \quad (11)$$

$$C_{NO_2-Pt} = C_v K_4 X_{NO_2,wc} \quad (12)$$

where C_v is the concentration of vacant active Pt sites, and was obtained by a site balance on the active Pt sites, given by Eq. (13).

$$C_{Pt,Active} = \theta_{Pt,Active} C_T \\ = C_v + C_{NO_2-Pt} + C_{O-Pt} + C_{NO-Pt} + C_{O_2-Pt} \quad (13)$$

It was reported that the concentration of adsorbed O₂ and NO₂ is negligible in comparison to the concentration of other surface species [7]. Hence, the terms corresponding to these species were neglected, resulting in Eq. (14), given as

$$C_v = \frac{C_{Pt,Active}}{1 + \frac{K_4 X_{NO_2,wc}}{K_3 K_1 X_{NO,wc}} + K_1 X_{NO,wc}} \quad (14)$$

On substituting the expression for C_v from Eq. (14) in Eqs. (11) and (12), the following expressions for concentrations of adsorbed O and NO₂ were obtained:

$$C_{O-Pt} = \frac{C_{Pt,Active} K_4 X_{NO_2,wc}}{\left[1 + \frac{K_4 X_{NO_2,wc}}{K_3 K_1 X_{NO,wc}} + K_1 X_{NO,wc} \right] K_3 K_1 X_{NO,wc}} \quad (15)$$

$$C_{NO_2-Pt} = \frac{C_{Pt,Active} K_4 X_{NO_2,wc}}{1 + \frac{K_4 X_{NO_2,wc}}{K_3 K_1 X_{NO,wc}} + K_1 X_{NO,wc}} \quad (16)$$

The expressions for C_{O-Pt} and C_{NO_2-Pt} from Eqs. (15) and (16), respectively, were used in Eqs. (10) and (9), respectively, to calculate the rate of reversible deactivation reactions, represented by (R6) and (R7). It is assumed that none of the species adsorbs on the inactive Pt_{Ox} and hence a site balance for the inactive sites was not written.

2.3. Numerical simulations

To solve the species balance equations, the monolithic channel was discretized in the axial direction to get a set of ordinary differential equations. These equations were integrated using ODE23s in

MATLAB®. The variation of inlet temperature with time was given as an input and the species balance equations were solved to get the spatio-temporal evolution of gaseous concentrations and the concentrations of active Pt sites. As described earlier, isothermal conditions were assumed and the temperature throughout the monolith was assumed to be the same as the inlet temperature. The simulation results were used to generate plots for NO conversion with respect to temperature for various temperature cycles. As the first step in the estimation of parameters, the kinetic parameters for NO oxidation reaction without considering deactivation were taken from Bhatia et al. [7]. To predict the experimental data reported by Hauptmann et al. [9], some of the kinetic parameters were modified while ensuring thermodynamic consistency. The parameters were changed since the catalysts used in the studies by Hauptmann et al. [9] and Bhatia et al. [7] were different. The values of rate parameters used in the present work are given in Table 2. A comparison of the kinetic parameters reported by Bhatia et al. [7] for the NO oxidation reaction without consideration of deactivation and those used in the current work is given in Table 3. Please note that the parameters which are the same as those in Bhatia et al. [7] are not given in the table.

The kinetic parameters for the deactivation reactions (R6) and (R7) were manually changed to obtain trends similar to the experimental data reported by Hauptmann et al. [9]. A sensitivity analysis was performed to find the parameters which strongly influenced the predicted NO conversion. It was found that the kinetic parameters for reaction (R6) strongly influenced the NO conversion whereas the effect of reaction (R7) kinetic parameters on the NO conversion was not that significant. The kinetic parameters of reaction (R7) influenced the fraction of PtO_x, especially at high temperatures, where the decomposition of Pt oxides was predicted. However, under these conditions, a change in the PtO_x fraction did not affect the NO conversion as the overall NO oxidation reaction was thermodynamically limited. The parameters for the

deactivation reactions are given in Table 2 and the results of the sensitivity analysis are given in “Appendix A: Sensitivity Analysis”. The values of activation energies E_{f6} and E_{b6} were reported to be 32 kJ/mol and 0 kJ/mol, respectively by Hauptmann et al. [9] in contrast to 69.6 kJ/mol and 7 kJ/mol reported in this work. A possible reason for the difference is that the deactivation kinetic scheme in the current work is not the same as that proposed by Hauptmann et al. [9]. We considered the formation of Pt oxides according to reactions (R6) and (R7), whereas only reaction (R6) was considered in their work. Hence, the kinetic parameters for reaction (R6) reported by them included the combined effect of O₂ and NO₂ whereas the individual effects are reported in the current work.

3. Thermodynamic consistency analysis

3.1. Methodology

The thermodynamic consistency analysis was performed by checking the enthalpic and entropic constraints for the various reactions. The basic equations used for the enthalpic and entropic analysis of an *i*th reaction are given by Eqs. (17) and (18), respectively.

$$\Delta H_i = E_{fi} - E_{bi} \quad (17)$$

$$\Delta S_i = R \ln \left(\frac{A_{fi}}{A_{bi}} \right) \quad (18)$$

As the first step to check enthalpic constraints, the summation of activation energies of the various microkinetic reactions was used to obtain the enthalpy change of reaction for the reaction obtained by a linear combination of the various microkinetic reactions, and is given by Eq. (19). ‘*r*’ in Eq. (19) represents the number of reactions which are used in the linear combination and *v_i* represents the multiplicative factor for the *i*th reaction.

$$\Delta H = \sum_{i=1}^r v_i (E_{fi} - E_{bi}) \quad (19)$$

The next step involved finding the product of the pre-exponential factors of the various steps in the microkinetic mechanism to obtain the entropy change of the reaction obtained by the linear combination of the various steps, and is represented by Eq. (20), as

$$\Delta S = R \ln \prod_{i=1}^r \left(\frac{A_{fi}}{A_{bi}} \right)^{v_i} \quad (20)$$

Using the values of the enthalpy and entropy change obtained from Eqs. (19) and (20), respectively, the Gibbs free energy change (ΔG) of the reaction was obtained using Eq. (21), as

$$\Delta G = \Delta H - T_s \Delta S \quad (21)$$

The Gibbs free energy change for the reaction was also calculated using gas phase thermochemistry data and compared to the value obtained from the above analysis [18].

A step wise approach was taken in which the thermodynamic consistency analysis was first performed for the NO oxidation reaction without considering the deactivation effects ((R1)–(R5)). This was followed by the thermodynamic analysis for the reactions which considered the reversible deactivation of Pt sites ((R6) and (R7)).

3.2. Analysis of NO oxidation reaction without deactivation

The activation energies and the pre-exponential factors of steps (R1)–(R5) are given in Table 2 and were used to calculate the Gibbs

Table 2
Values of microkinetic parameters used in the simulations.

Parameter	Numerical value	Parameter	Numerical value (kJ/mol)
A _{f1}	$7.50 \times 10^9 \text{ mol/m}^3 \text{ washcoat-s}$	E _{f1}	0
A _{f2}	$4.04 \times 10^4 \text{ mol/m}^3 \text{ washcoat-s}$	E _{f2}	0
A _{f3}	$4.5 \times 10^{14} \text{ mol/m}^3 \text{ washcoat-s}$	E _{f3}	98.3
A _{f4}	$7.2 \times 10^9 \text{ mol/m}^3 \text{ washcoat-s}$	E _{f4}	0
A _{f5}	$5.93 \times 10^{18} \text{ mol/m}^3 \text{ washcoat-s}$	E _{f5}	77.4
A _{f6}	$1.04 \times 10^9 \text{ s}^{-1}$	E _{f6}	69.6
A _{f7}	$2.66 \times 10^{-1} \text{ s}^{-1}$	E _{f7}	37.5
A _{b1}	$1.27 \times 10^{16} \text{ mol/m}^3 \text{ washcoat-s}$	E _{b1}	110.3
A _{b2}	$2.04 \times 10^{13} \text{ mol/m}^3 \text{ washcoat-s}$	E _{b2}	62.4
A _{b3}	$4.78 \times 10^{14} \text{ mol/m}^3 \text{ washcoat-s}$	E _{b3}	44.9
A _{b4}	$5.7 \times 10^{17} \text{ mol/m}^3 \text{ washcoat-s}$	E _{b4}	97.9
A _{b5}	$1 \times 10^{22} \text{ mol/m}^3 \text{ washcoat-s}$	E _{b5}	209.4
A _{b6}	$1 \times 10^{11} \text{ s}^{-1}$	E _{b6}	7
A _{b7}	$1.81 \times 10^{13} \text{ s}^{-1}$	E _{b7}	193.2

Table 3
Comparison of kinetic parameters with literature.

Parameter	Current work	Values from Bhatia et al. [7]
A _{f2}	$4.04 \times 10^4 \text{ mol/m}^3 \text{ washcoat-s}$	$1.41 \times 10^5 \text{ mol/m}^3 \text{ washcoat-s}$
A _{f4}	$7.2 \times 10^9 \text{ mol/m}^3 \text{ washcoat-s}$	$8.0 \times 10^9 \text{ mol/m}^3 \text{ washcoat-s}$
A _{f5}	$5.93 \times 10^{18} \text{ mol/m}^3 \text{ washcoat-s}$	$4.94 \times 10^{18} \text{ mol/m}^3 \text{ washcoat-s}$
A _{b2}	$2.04 \times 10^{13} \text{ mol/m}^3 \text{ washcoat-s}$	$1.74 \times 10^{13} \text{ mol/m}^3 \text{ washcoat-s}$
A _{b3}	$4.78 \times 10^{14} \text{ mol/m}^3 \text{ washcoat-s}$	$2.5 \times 10^{14} \text{ mol/m}^3 \text{ washcoat-s}$
E _{f3}	98.3 kJ/mol	101.3 kJ/mol
E _{f5}	77.4 kJ/mol	80 kJ/mol
E _{b1}	110.3 kJ/mol	106.9 kJ/mol
E _{b2}	62.4 kJ/mol	80 kJ/mol

free energy change for the NO oxidation reaction using Eqs. (17)–(21). The calculated value was found to be the same as the Gibbs free energy change obtained using gas phase thermochemistry data at 25 °C [19]. At higher temperatures, there was a slight deviation in the Gibbs free energy values obtained from kinetic parameters and those obtained from gas phase data. This is because the thermodynamic parameters predict a dependence of temperature on the enthalpy and entropy change of a reaction. However, the activation energies and pre-exponential factors are assumed to be independent of temperature in the kinetic model, thus resulting in a slight difference in the two values with an increase in temperature.

3.3. Analysis of deactivation reactions

Reaction (R7) involves chemisorbed oxygen and formation of Pt oxides and the Gibbs free energy change for this step is not directly known. Hence, the approach was to consider a series of reactions, a linear combination of which resulted in a reaction for which the thermodynamic values are reported in the literature. It was observed that a linear combination of reactions (R2), (R5) and (R7) resulted in reaction (R8), which involved the formation of Pt oxides from Pt and gas phase oxygen.



Taking the approach discussed in Section 3.1, the Gibbs free energy of reaction (R8) was obtained by using the kinetic parameters of reactions (R2), (R5) and (R7). This was then compared to the Gibbs free energy of formation of Pt oxides reported by Seriani et al. [20]. The limitation to this analysis is that the deactivation model proposed by us does not consider explicitly if the species formed is PtO or PtO₂, i.e., the fraction of either oxide formed is unknown. Hence, a comparison of the Gibbs free energy change obtained for the following three cases is compared: (i) reported value for PtO formation ($\Delta G_{\text{PtO}}^{\text{thermo}}$) [20], (ii) reported value for PtO₂ formation ($\Delta G_{\text{PtO}_2}^{\text{thermo}}$) [20] and (iii) calculation using kinetic parameters ($\Delta G^{\text{kin},7}$). A comparison of the three cases is given in Table 4. It is observed that the calculated values of Gibbs free energy change are in between the values reported for only PtO or only PtO₂ formation. This indicates that the kinetic parameters used in the current simulations are within the expected range. A similar strategy was employed to analyze the thermodynamic consistency of the kinetic parameters of reaction (R6). It was observed that a linear combination of reactions (R1)–(R3), (R5) and (R6) resulted in reaction (R8). Hence, the kinetic parameters of reactions (R1)–(R3), (R5) and (R6) were used to obtain the Gibbs free energy change for reaction (R8) ($\Delta G^{\text{kin},6}$) and are given in Table 4. It is observed that for all the temperatures studied, the calculated Gibbs free energy change for reaction (R8) is in between the values reported for only PtO and PtO₂ formation [20]. Thus, the kinetic parameters used in the current work are within the expected range.

Table 4

Comparison of calculated Gibbs free energy change with reported values at various temperatures.

Temperature (°C)	$\Delta G_{\text{PtO}}^{\text{thermo}}$ (kJ/mol)	$\Delta G_{\text{PtO}_2}^{\text{thermo}}$ (kJ/mol)	$\Delta G^{\text{kin},7}$ (kJ/mol)	$\Delta G^{\text{kin},6}$ (kJ/mol)
100	-61.6	-124.2	-120.9	-66.5
200	-35.9	-105.7	-83.5	-59.5
300	-10.2	-87.3	-46.1	-52.5
400	0.015	-68.8	-8.7	-45.5

4. Results

4.1. Inverse hysteresis during oxidation of NO at 450 ppm concentration

For the experiments conducted by Hauptmann et al. [9], a stream of reactant gases consisting of 450 ppm NO, 6% O₂ and remaining N₂ was passed through the monolith. The temperature of the reactant stream was ramped from 80 °C to 370 °C at a ramp rate of 5 °C/min and then ramped down to 80 °C at the same rate. This program was performed twice, one after the other, without stopping the experiment. We refer to the first set of experiments (including increasing and decreasing temperature ramp) as run 1 and the next set of experiments as run 2.

Fig. 2(a) shows the comparison between NO conversion predicted by our model and the experimental data reported by Hauptmann et al. [9]. The equilibrium NO conversion is also plotted for reference. It is observed that the modelling results follow the same trend as the experimental data and the numerical values match closely during the temperature ramp-up. As the temperature increases, NO conversion increases monotonically till a temperature of ~160 °C because of an increase in the reaction rate. Since NO oxidation is an exothermic reaction, the NO conversion decreases with a further increase in temperature because of thermodynamic limitations. As the temperature is ramped-down, the conversion increases again, but only till ~250 °C, after which it decreases monotonically until the end-temperature of 80 °C is

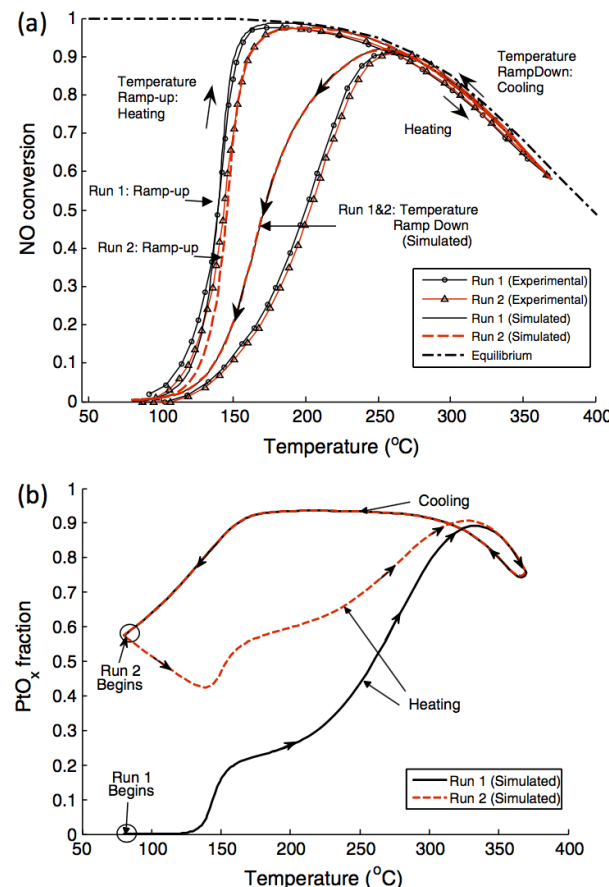


Fig. 2. (a) Comparison between experimental and simulated NO conversion for first and second run with 450 ppm NO, 6 vol.% O₂ and balance N₂. (b) Simulated results for platinum oxide fraction for first and second run under the same conditions.

reached. Between 80 °C and 250 °C, NO conversion during temperature ramp-down is lower than that obtained during temperature ramp-up, a phenomenon believed to occur because of the deactivation of Pt sites. With the start of run 2, it is observed that the NO conversion is slightly less than that observed in run 1. The model-predicted light-off temperature, defined as the temperature at which 50% NO conversion takes place, is 139.2 °C and 144.9 °C for run 1 and run 2, respectively. This is in close agreement with the light-off temperatures of 138 °C and 143 °C, obtained for the experiments performed by Hauptmann et al. [9].

For both run 1 and run 2, the ramp-up NO conversions closely match the experimental data. It is also observed that the model-predicted NO conversion during ramp-down is less than that during the ramp-up, which is in agreement with the experimental data. It is predicted that the NO conversion profile during temperature ramp-down is nearly the same for run 1 and run 2, which is also observed from the experimental data. However, the model-predicted NO conversion during temperature ramp-down is more than the experimental NO conversion, especially below 250 °C, even though the final restoration of activity is correctly predicted by the model, which can be seen from the experimental and model-predicted light-off behavior during the temperature ramp-up of run 2. The difference between model-predicted results and experimental data during ramp-down indicates that the model overestimates the rate of restoration of Pt activity by the reduction of Pt oxides. This can be assessed by analysing our assumption of uniform catalyst deactivation throughout the washcoat. Hauff et al. [15] proposed that a protective surface oxide layer could form, preventing diffusion of oxygen into the bulk of platinum. The occlusion of Pt sites and/or the enhanced restriction in the transport of gases, both brought about by formation of PtO_x, is not considered in the present model and could explain the overestimation of NO conversion during temperature ramp-down. This is because during the temperature ramp-down, there could be some active Pt sites, which are not available to reactant gases and hence cause low NO conversions observed during the experiments. Because of the lack of understanding related to steric effects and their impact on diffusional limitations, this phenomenon has not been included in our model, and hence a uniform concentration of deactivated Pt sites in the transverse direction is assumed.

Fig. 2(b) shows the variation of fraction of inactive sites with temperature for the same experimental conditions as those for Fig. 2(a). It is assumed that at the beginning of run 1, all the Pt sites are active, i.e., the fraction of inactive sites is zero. It is observed that the fraction of inactive Pt sites is almost zero for temperatures below ~125 °C owing to a low deactivation rate. With a further increase in temperature, the fraction of inactive Pt sites increases monotonically till ~340 °C owing to an increase in oxidation of Pt sites by NO₂ and O₂, which outweighs the reduction rate by NO. The model parameters are such that the rate of oxidation of Pt sites by NO₂ is higher than the rate of oxidation by O₂, despite the lower concentration of NO₂ [4,7]. As the temperature increases further, the activity of the catalyst is regained because of thermal decomposition of platinum oxides, represented by the reverse reaction (R7). This is in accordance with the findings by Hauff et al. [15], who proposed that Platinum oxide decomposes to Pt at temperatures exceeding 350 °C. Olsson and Fridell [9] reported a more pronounced activity decrease of the NO oxidation reaction over a Pt/Al₂O₃ catalyst at 250 °C than at 300 °C. This could be explained by the decomposition of Pt oxides at high temperatures, which results in low deactivation rates. The XPS data reported by Peuckert and Bonzel [12] also showed the thermal decomposition of Pt oxides at high temperatures.

During the temperature ramp-down experiment, the thermal decomposition rate of oxidized Pt sites decreases relative to the platinum oxidation rate, resulting in an increase in the fraction of

inactive Pt sites till ~200 °C. Below 200 °C, the presence of NO results in the reactivation of platinum sites, which decreases the fraction of inactive Pt sites to 0.58 at the end temperature of the ramp-down experiment, i.e. 80 °C. This is in accordance with the findings of Hauff et al. [15]. The catalyst is again subjected to the same temperature program as run 1, with the initial conditions same as that obtained at the end of run 1, and is termed as run 2.

From Fig. 2(a), it is observed that during the temperature ramp-up of run 2, NO conversion follows a 'low conversion path' in comparison to run 1 ramp-up. This is because of the deactivated state of some Pt sites. However, during temperature ramp-down, the conversion follows the same path as that followed by run 1 temperature ramp-down. Also, the curve for the fraction of inactive Pt sites for run 1 ramp-down nearly overlaps with that of run 2 ramp-down. This is because of the reversible and near-equilibrium thermal decomposition of inactive Pt sites at temperatures exceeding ~320 °C. Due to this, the number of deactivated Pt sites at the beginning of run 2 ramp-down experiments are nearly independent of the history during the temperature ramp-up and are nearly the same as that at the beginning of run 1 ramp-down.

It is observed that even though the fraction of inactive sites is high (≈ 0.58) at the beginning of temperature ramp-up of run 2, the conversion is only slightly below that obtained during run 1. To check the accuracy of our results, a simulation was performed to study the variation of steady state NO conversion with temperature for various catalyst loadings. For these simulations, the deactivation and reactivation effects were not considered and the results are shown in Fig. 3. It is observed that the light-off temperature does not vary linearly with catalyst loading. As the platinum active site concentration is lowered by a factor of 100 from the base value of 40 mol/m³ to 0.4 mol/m³, the light-off temperature increases from 139 °C to 235 °C, i.e., a change by a factor of only 1.23 calculated in SI units. This observation gives credence to our simulation result that despite the fraction of inactive Pt sites being as high as 0.58 at the beginning of run 2, the conversion during run 2 ramp-up is only slightly lower than the conversion obtained during run 1 ramp-up.

4.2. Inverse hysteresis during oxidation of NO at 300 ppm concentration

The inverse hysteresis experiment was performed by Hauptmann et al. [9] for an inlet concentration of 300 ppm, with other

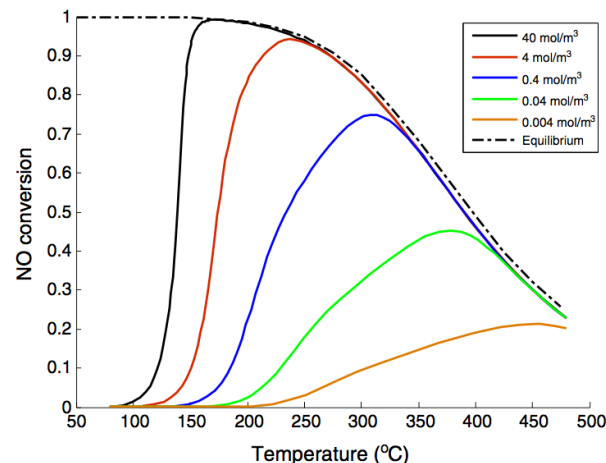


Fig. 3. Effect of catalyst loading on light-off behavior for NO oxidation.

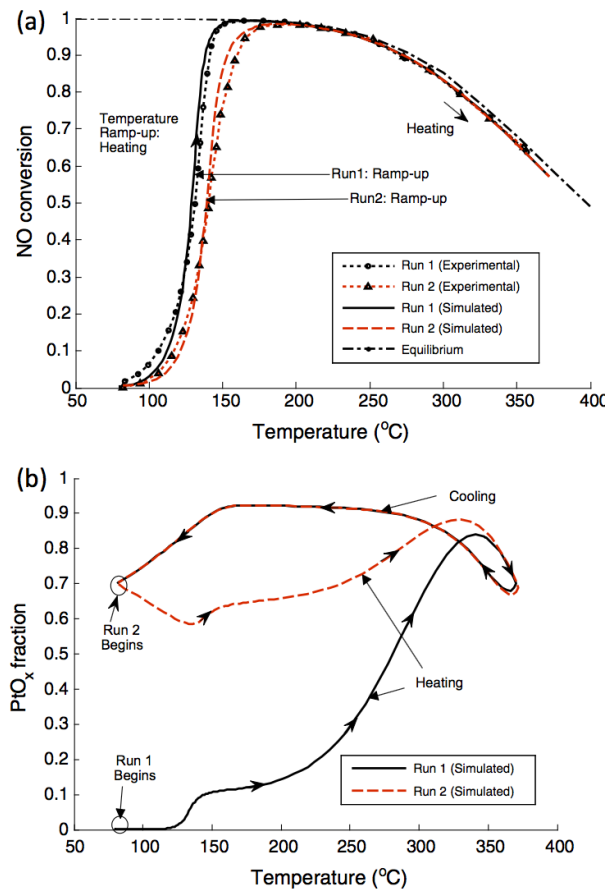


Fig. 4. (a) Comparison between experimental and simulated NO conversion for the temperature ramp-up of first and second run with 300 ppm NO, 6 vol.% O₂ and balance N₂. (b) Simulated results for platinum oxide fraction under same conditions.

conditions and procedure being the same as those given in Section 4.1. Fig. 4(a) shows a comparison between the model-predicted NO conversion and experimental data reported by Hauptmann et al. [9] during temperature ramp-up for an inlet NO concentration of 300 ppm. The model-predicted fraction of inactive sites is shown in Fig. 4(b). A similar match of simulated and experimental trends is seen in Fig. 4(a) as was observed with 450 ppm NO concentration. In this case, a lower concentration of NO leads to a lower concentration of NO₂. This leads to a comparatively lower fraction of inactive Pt sites, which reaches a maximum of 0.83 and 0.88 during temperature ramp-up of run 1 and run 2, respectively, in comparison to 0.88 and 0.90 for the case of higher NO concentration (=450 ppm). Secondly, lower concentration of NO leads to a weakened reactivation of the inactive sites, which is observed by comparing Fig. 2(b) and Fig. 4(b). During

the temperature ramp-down of run 1, the fraction of inactive Pt sites reduces from a peak value of 0.92 to 0.70 for 300 ppm NO, whereas the decrease is much larger (0.94–0.58) in the case of high NO concentration (=450 ppm).

4.3. Light-off temperature

The light-off temperature, defined as the temperature at which NO conversion reaches 50%, was calculated using experimental data and modelling results for various experiments. Table 5 shows the comparison between experimental light-off temperature data and model-predicted results. The first three experiments show the impact of inlet NO concentration on the light-off characteristics for fixed values of gas hourly space velocity and temperature ramp rate. It is observed that as the concentration of NO increases from 150 ppm to 450 ppm, the model-predicted light-off temperature increases from 111.9 °C to 139.2 °C. The increase in light-off temperature with an increase in NO concentration suggests that the effective order of the NO oxidation reaction with respect to NO is less than 1. It was shown by Bhatia et al. [7] that at low temperatures, NO adsorbs strongly on the catalyst surface and inhibits the reaction. This is in accordance with our results of high NO concentrations increasing the light-off temperature. It is observed that the light-off temperatures for both run 1 and run 2 are predicted closely by the model for all the three inlet NO concentrations.

The effect of space velocity on the light-off temperature is seen by comparing rows 2 and 4 of Table 5. It is observed that both the experimental and simulated light-off temperatures increase with an increase in space velocity for run 1 as well as run 2. This can be explained by the decrease in the gas residence time with an increase in space velocity. Hence, higher temperatures are required at high space velocities to attain the same levels of conversion.

The effect of temperature ramp-rate on the light-off temperature is seen by comparing rows 3 and 5 of Table 5. It is observed that there is a slight decrease in the light-off temperature when a high ramp rate is used. This could be because the catalyst is exposed to oxidizing gases, viz., O₂ and NO₂ for a shorter duration. On the other hand, a slight increase in the light-off temperature during run 2 with a high ramp rate could be because of the reduction in time for which the catalyst is exposed to the reducing NO environment during run 1 ramp-down.

4.4. 3-cycle temperature program

An experiment consisting of 3 temperature cycles with various beginning and end temperatures was performed by Hauptmann et al. [9] and is described as follows: First, the monolith channel was regenerated by heating it at 370 °C for an hour under N₂ atmosphere to reduce any inactive Pt sites. Then, a stream of reactant gases consisting of 450 ppm NO, 6% O₂ and N₂ as carrier gas was passed through the monolith reactor. The temperature program was set as follows: in run 1, the temperature was ramped up at 5 °C/min from 80 °C to 270 °C, and then ramped down to 120 °C; in run 2, the temperature was ramped up from 120 °C to 370 °C,

Table 5
Comparison between experimental and model-predicted light-off temperatures.

S. no.	NO concentration (ppm)	Ramp rate (°C/min)	GHSV (h ⁻¹)	Light-off temperature for run 1 (°C)		Light-off temperature for run 2 (°C)	
				Experiment [9]	Simulated	Experiment [9]	Simulated
1	150	5	25,000	113	111.9	127	125.1
2	300	5	25,000	131	128.8	140	138.9
3	450	5	25,000	138	139.2	143	144.9
4	300	5	50,000	141	137.1	151	147.2
5	450	10	25,000	137	138.9	144	149.5

and then ramped down to 120 °C; finally, in run 3, the temperature was ramped up to 270 °C, and then ramped down to 80 °C. All these runs were programmed such that the ramp rate was the same (5 °C/min) throughout, without any delay in between the three runs.

Fig. 5(a) and (b) shows the comparison between the experimental data and model-predicted NO conversion for the 3-cycle temperature program. The experimental and modelling results are

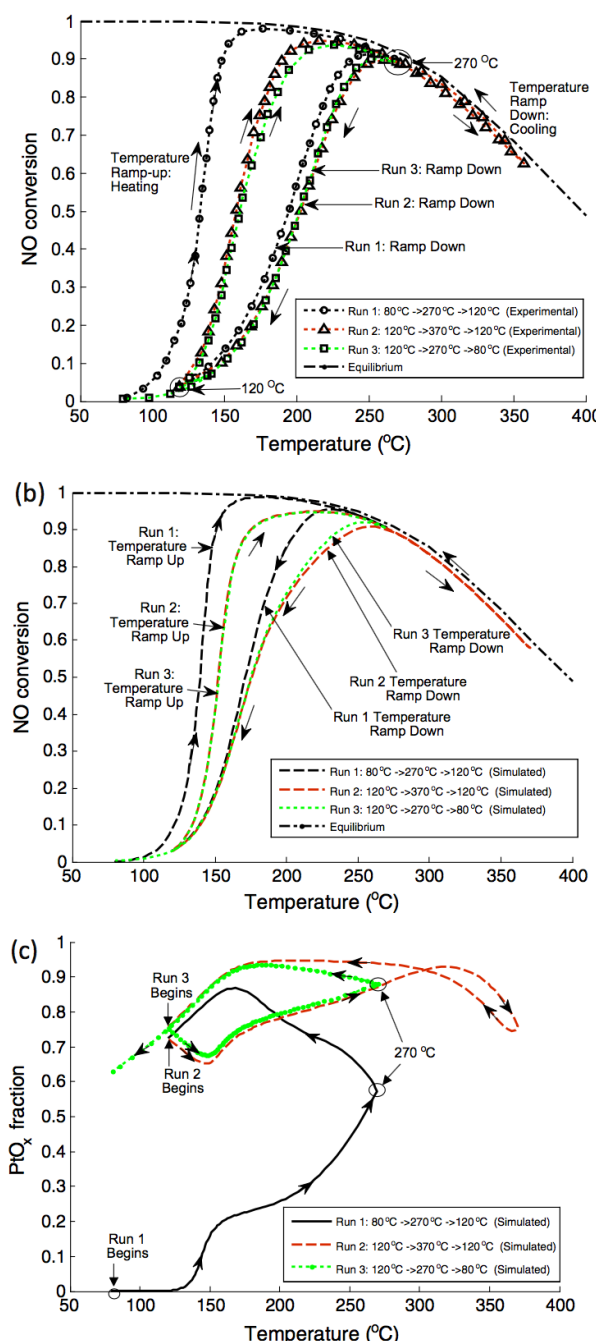


Fig. 5. (a) Experimental NO conversion data for 3-cycle temperature program with 450 ppm NO, 6 vol.% O₂, and balance N₂. (b) Simulated NO conversion results for 3-cycle temperature program for the same conditions. (c) Simulated results for platinum oxide fraction for the 3-cycle temperature program under same conditions.

shown in separate figures for legibility. It is observed from **Fig. 5(a)** that the NO conversion for run 1 is similar to that in **Fig. 2(a)**, which consists of a temperature ramp-up from 80 °C to 370 °C, followed by a temperature ramp-down back to 80 °C. It is also observed from **Fig. 5(a)** that the NO conversion shows a similar trend for run 2 and run 3, for both the positive and negative temperature ramps. This is also predicted by the simulation results, as observed in **Fig. 5(b)**. The NO conversion during the temperature ramp-up for run 2 in the 3-cycle program is lower than that for run 2 shown in **Fig. 2(a)**. This suggests that at the start of run 2 of the 3-cycle temperature program, the fraction of active Pt sites is lower than that at the start of run 2 of the single cycle temperature program. This also suggests a lower degree of reactivation during run 1 temperature ramp-down in the present case in which temperature is ramped down to 120 °C, as against the single temperature cycle when the temperature was ramped down to 80 °C. This indicates that reactivation of the Pt sites takes place effectively at lower temperatures. This trend is also predicted by the model, as shown in **Fig. 5(b)**.

To corroborate the analysis, the fraction of inactive Pt sites is plotted in **Fig. 5(c)** for the 3-cycle temperature program. It is observed that at the beginning of run 2, the fraction of inactive sites is 0.72 whereas for the single temperature cycle, the value was 0.58 at the beginning of run 2. This shows that reactivation is favored at low temperatures. One could argue that the higher fraction of inactive sites in the current case could be because of the difference in the peak temperatures during the temperature ramp-up of run 1. However, it can be observed from **Fig. 2(b)** that when the peak temperature during run 1 ramp-up is high (=370 °C), the fraction of inactive sites is even higher at 270 °C (=0.92) during the temperature ramp-down as compared to the value obtained at the same temperature at the beginning of run 1 temperature ramp down (=0.58) in the 3-cycle program. This shows that the temperature plays a key role in the reactivation of the catalyst, with low temperatures favoring reactivation.

To understand the role of temperature in reactivation during the temperature ramp-down, simulations were performed for the same conditions as in **Fig. 2(a)**, except for the end-temperature at which run 1 ramp-down is stopped. During run 1, the temperature was ramped up to 370 °C followed by a ramp-down to a specific temperature, which was varied for different simulations. This was followed by another temperature ramp-up to 370 °C to elucidate the effect of end-temperature of run 1 on the NO conversion of the subsequent run, i.e., run 2. The variation of NO conversion with temperature for the ramp-up of run 2 for various end-temperatures of run 1 is shown in **Fig. 6**. For comparison, NO conversion during the temperature ramp-up and ramp-down of run 1 is also shown for the base case, i.e., when the end-temperature during ramp-down of run 1 is 80 °C. It is observed that as the end-temperature of run 1 is increased from 80 °C to 160 °C, the NO conversion in the subsequent ramp-up decreases. This shows that reactivation of the catalyst takes place efficiently at lower temperatures. This is in agreement with the experimental data reported by Hauff et al. [15]. This result can be related to the experimental data shown in **Fig. 5(a)** where a higher value of the temperature at the end of run 1 ramp-down (=120 °C) in comparison to that in **Fig. 2(a)** (= 80 °C) is responsible for the reduced NO conversion during the temperature ramp-up of run 2.

From **Fig. 5(a)**, it is observed that the NO conversion during run 1 ramp-down starts to decrease at a lower temperature (~230 °C) than in run 2 and run 3 ramp-downs, where it starts decreasing at ~260 °C. This is also predicted by the kinetic model, as seen in **Fig. 5(b)** and explained by the higher coverage of inactive sites at the end of ramp-up of run 2 (=0.74) and run 3 (=0.88), as compared to that at the end of ramp-up of run 1 (=0.58). The lower value of the fraction of inactive sites at the end of run 1 ramp-up as com-

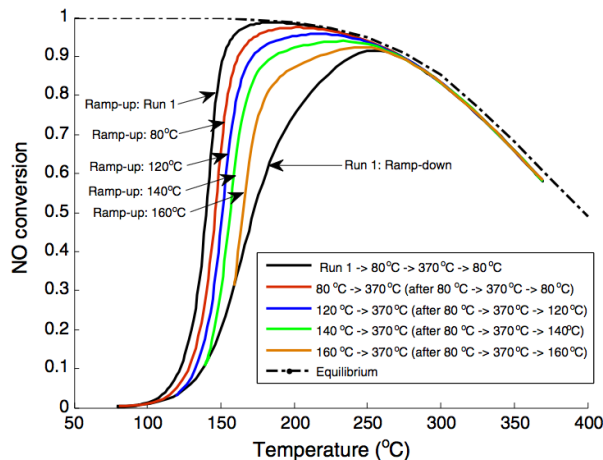


Fig. 6. Variation of NO conversion with temperature during run 2 for various values of end-temperature of run 1 (reaction mixture: NO = 450 ppm, O₂ = 6% and balance N₂; ramp rate = 5 °C/min).

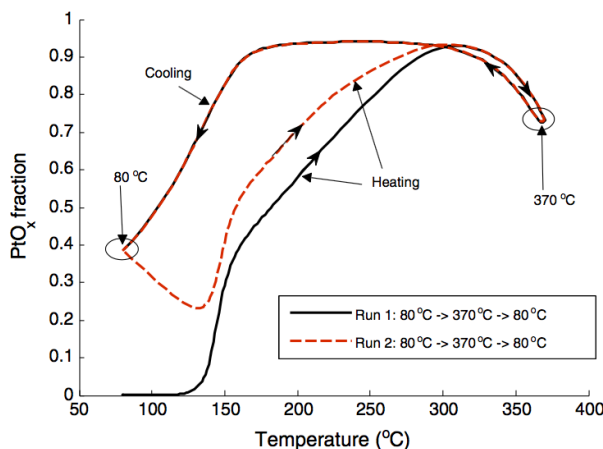


Fig. 7. Variation of fraction of inactive sites with temperature for a reduced ramp rate of 2.5 °C/min (reaction mixture: NO = 450 ppm, O₂ = 6% and balance N₂).

pared to that of run 2 is because of the lower value of peak temperature (270 °C) in run 1 as compared to the peak temperature (370 °C) in run 2. The kinetic limitations prevented the fraction of inactive Pt from reaching its equilibrium value. Moreover, in the present cycle, at the beginning of temperature ramp in run 1, the fraction of inactive sites is zero, whereas a residual fraction of inactive sites (0.72) exists at the beginning of the temperature ramp of run 2, which results in the increase in inactive sites for the subsequent cycles. As discussed earlier, this residual fraction is high also because the temperature was ramped down only till 120 °C, which caused a limited degree of reactivation. Another thing worth noting is that at a ramp rate of 5 °C/min, the total time available for each run is limited. Had the rate been lower than 5 °C/min, there would have been more time available for both the deactivation and reactivation of the catalyst. This was confirmed by a simulation with a ramp rate of 2.5 °C/min, with all other conditions the same as those in Fig. 2(a). The dependence of temperature on the fraction of inactive sites for the reduced ramp rate is shown in Fig. 7. It is observed that for any given temperature less than ~330 °C, the fraction of inactive sites during ramp-up is higher

for the ramp-rate of 2.5 °C/min, as compared to those in Fig. 2(b) for the ramp rate of 5 °C/min. However, at high temperatures, the increase in rates for thermal decomposition result in similar fraction of inactive sites for both the ramp rates. Also, it is observed that at the beginning of run 2, the fraction of inactive sites is 0.39, which is less than that obtained with the higher ramp-rate in Fig. 2(b). This can again be related to the increased time of exposure to the reactivating environment for a lower temperature ramp rate.

To summarize, it can be concluded from the experimental data and modelling results that the deactivation of catalyst and the regain in activity (referred to as reactivation in the current work) results in the observed phenomenon of inverse hysteresis. In the present work, it is observed that between ~140 °C and ~280 °C, the rate of deactivation is high and that it dominates over the rate of reactivation whereas the opposite effect is observed for temperatures below 140 °C and above ~300 °C. Both the peak temperature during temperature ramp-up and the end-temperature during temperature ramp-down affect the deactivation and reactivation of the catalyst, resulting in different NO conversion trends for different cycles.

4.5. Effect of peak temperature during ramp-up

For the 3-cycle temperature program discussed in Section 4.4, it was observed from Fig. 5(a) that the NO conversion during ramp-down was similar for run 2 and run 3, despite a difference of 100 °C between the peak temperatures at the end of ramp-up. Also, the NO conversion during ramp-down was different for run 1 and run 3, despite the equal value of peak temperatures at the end of ramp-up for both these runs. Hence, we performed a sensitivity analysis to study the effect of peak temperature at the end of ramp-up on NO conversion during the corresponding ramp-down. Four independent simulation runs were performed in which the temperature was ramped up from 80 °C to a particular peak temperature, which was varied for the four different runs. Once the peak temperature was reached, the temperature was reduced to 80 °C at the same ramp rate of 5 °C/min. The fraction of inactive sites at the start of each run was assumed to be zero. The NO conversion for the four different runs during the ramp-down is shown in Fig. 8. It is observed that an increase in the peak ramp-up temperature from 180 °C to 310 °C (run 4 to run 2) results in a decrease in NO conversion at a given temperature during the ramp-down. This is because of an increase in the formation of Pt oxides with temperature during the ramp-up. It is also observed that the NO

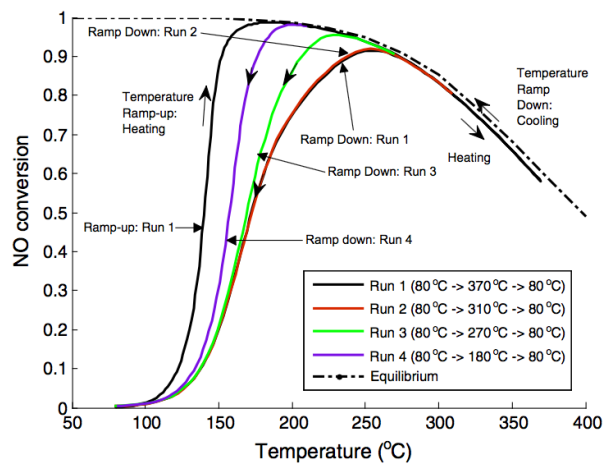


Fig. 8. Effect of temperature at the end of ramp-up on the NO conversion during subsequent ramp-down (reaction mixture: NO = 450 ppm, O₂ = 6% and balance N₂; ramp rate = 5 °C/min).

conversion during the ramp-down of run 1 and run 2 is nearly the same. This is attributed to the fast decomposition of Pt oxides at high temperatures and the near equilibrium conditions for reaction (R7), due to which the amount of Pt oxides is nearly the same at ~310 °C, irrespective of whether this temperature is attained during the temperature ramp-up or ramp-down.

4.6. Effect of cooling under different gas compositions

Simulations were performed to study the effect of composition of gas mixture during ramp-down on the NO conversion during the subsequent ramp-up, and the results are shown in Fig. 9 for 4 different conditions. Run 1 in the figure is the same as that shown in Fig. 2(a) and represents the base case, in which the ramp-up and ramp-down are done in the presence of the reaction mixture consisting of 450 ppm NO, 6% O₂ and remaining N₂. For the other three runs, the temperature was ramped up from 80 °C to 370 °C in the reaction mixture, similar to run 1. This was followed by a decrease in temperature to 150 °C under different gas compositions, and finally, the temperature was ramped up again to 370 °C in the reaction mixture consisting of 450 ppm NO, 6% O₂ and remaining N₂. The variation of NO conversion with temperature during the second temperature ramp-up is shown in Fig. 9. For run 2, the cooling was performed under reaction conditions given above, whereas run 3 involved cooling in N₂. It is observed that the NO conversion for run 2 is lower than that of run 1. This is because as shown in Fig. 6 and discussed in Section 4.4, high temperatures at the end of a ramp-down result in a limited reactivation. For run 3 involving cooling in N₂, it is observed that the NO conversion is nearly the same as that during the ramp-up during run 1. This can be explained by the enhanced reactivation of the catalyst in the absence of oxidizing species such as NO₂, which shifts the equilibrium of reaction (R7) in the reverse direction. For run 4, the cooling was done in the reaction mixture till 300 °C followed by cooling in a pure N₂ atmosphere. It is observed that the reactivation did not take place effectively. This can be explained by the increase in Pt oxides with a decrease in temperature till 300 °C under reaction conditions, as was also shown in Fig. 2(b) for the ramp-down. With a further reduction in the temperature, the reactivation did not occur due to the absence of NO, which could reduce the Pt oxides to the active form. Additionally, even though not shown here, it was observed that at temperatures lower than 300 °C, the reactivation of the catalyst did not take place by thermal decomposition of the Pt oxides. The model-predicted effect of cooling under different

conditions is consistent with Hauff et al. [13,15], who reported that cooling in N₂ from a high temperature resulted in activity similar to the first temperature ramp. They also reported that partial cooling in reaction mixture followed by cooling in N₂ results in lower NO conversions as compared to the case in which the entire cooling is done under a N₂ atmosphere. Hauff et al. [15] argued that when the cooling is performed under a N₂ atmosphere, the fraction of inactive Pt sites will remain unchanged. However, the thermal decomposition of Pt oxides can take place even in the absence of the reaction mixture, a result which is also predicted by our simulations. The reversible nature of Pt oxides formation is considered in reaction (R7) and is able to predict the trends in the experimental data reported by Hauff et al. [15].

4.7. Effect of holding time for various gas compositions

The inverse hysteresis phenomenon shown in Fig. 2(a) consisted of a continuous change in the temperature, i.e., there was no time delay between the end of ramp-down and the beginning of the subsequent ramp-up. We performed independent simulations to find the effect of maintaining a constant temperature for a fixed time before the start of the next temperature ramp-up. For the various runs, the temperature was ramped up from 80 °C to 370 °C, followed by a decrease in temperature to 140 °C in the reaction mixture. The temperature was then held constant at 140 °C and the catalyst was exposed to three different gas compositions for 30 min for three different independent runs. The temperature was ramped up again to 370 °C in the reaction mixture consisting of 450 ppm NO, 6% O₂ and remaining N₂. All these runs were performed independent of each other, and the catalyst was assumed to be completely active at the start of each independent run.

The simulation results for the second temperature ramp-up for various fixed gas compositions are shown in Fig. 10. Run 1 shown in the figure is the same as in Fig. 2(a) and represents the base case. Run 3 involved exposing the catalyst to NO for 30 min and it is observed that the NO conversion is similar to that of run 1. This is because of the presence of NO for an extended duration, which results in reactivation of the catalyst. In run 2, the catalyst was exposed to a mixture of 450 ppm NO and 6% O₂, which also resulted in the reactivation. However, the degree of reactivation is less as compared to when only NO is present. This is because the presence of O₂ and the formation of NO₂ from NO and O₂, which contribute to the formation of Pt oxides, thus reducing the overall extent of reactivation. However, the NO conversion during

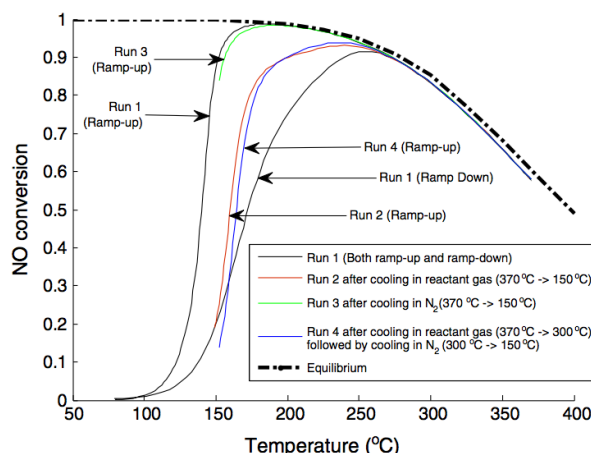


Fig. 9. Effect of cooling under different conditions on the hysteresis curve (reaction mixture: NO = 450 ppm, O₂ = 6% and balance N₂; ramp rate = 5 °C/min).

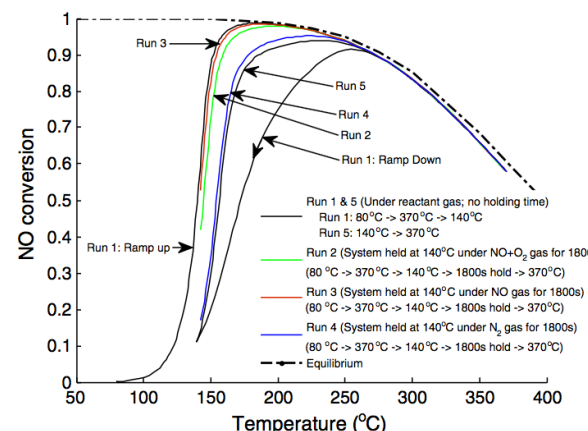


Fig. 10. Effect of holding time on NO conversion under different gas compositions (reaction mixture: NO = 450 ppm, O₂ = 6% and balance N₂; ramp rate = 5 °C/min).

run 2 is more than the case in which the temperature was not held fixed but was increased immediately after reaching the temperature of 140 °C, as represented by run 5. This is because in run 2, the catalyst is exposed to the reaction mixture responsible for reactivation at low temperatures for a higher duration of time. As discussed in Section 4.4 and shown in Fig. 6, low temperatures favour the reactivation of the catalyst. Hence, exposing the catalyst to the reaction mixture at low temperatures for longer periods results in reduction in the amount of Pt oxides and an increase in NO conversion for the subsequent ramp-up. For run 4, the catalyst was exposed to N₂ only and it is observed that the NO conversion during the subsequent ramp-up is significantly less than that in runs 2 and 3. This is because of the absence of NO under conditions of run 4, which is primarily responsible for the reactivation at low temperatures. Also, it is observed that the NO conversion for run 4 is slightly higher than that for run 5. The results for the effect of holding the temperature constant for various gas compositions are in agreement with those reported by Hauff et al. [15].

Bhatia et al. [7] developed a kinetic model for NO oxidation over a Pt/Al₂O₃ catalyst. Even though they reported the loss in catalyst activity with time-on-stream, it was not considered in their model. Using the model developed in the present work, we performed simulations to predict the transient evolution of NO conversion for various catalyst temperatures under isothermal conditions and fixed inlet concentrations. For all these simulations, it was assumed that all the Pt sites are in the active form at the beginning of each run. The variation of NO conversion with time for various temperatures is shown in Fig. 11. It is observed that at low fixed temperatures ($=110$ °C), the NO conversion is essentially unchanged with time. If the reaction is performed at higher temperatures, the NO conversion decreases with time and the decrease in activity is spread over a larger time interval, e.g., at 130 °C, a steady state is achieved in ~ 1.5 h, whereas, at 190 °C, a steady state is achieved after 3.5 h. With a further increase in temperature, the decrease in activity is not observed, as near-equilibrium conditions are reached. These results are in agreement with Bhatia et al. [7], who reported that for low and high temperatures, a steady state is achieved in a few minutes whereas for intermediate temperatures, it takes a few hours to reach a steady state. Thus, the model developed in the current work is able to predict the different trends in the deactivation of the catalyst with time for various fixed temperatures.

The change in NO conversion with time-on-stream can also be analyzed by plotting the NO conversion after exposing the catalyst to the reaction mixture for a few hours at a fixed temperature. The

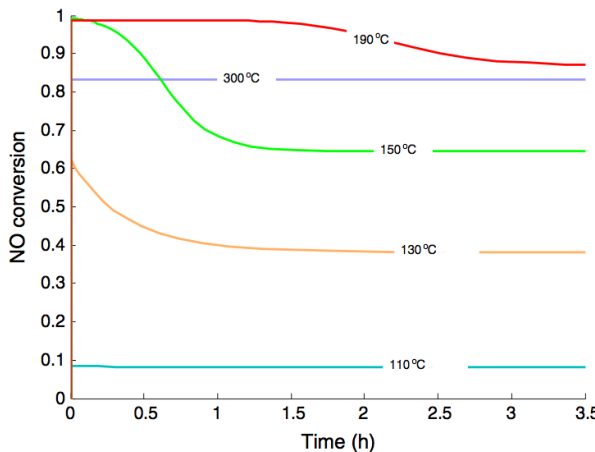


Fig. 11. Variation of NO conversion with time at different reaction temperatures (reaction mixture: NO = 450 ppm, O₂ = 6% and balance N₂).

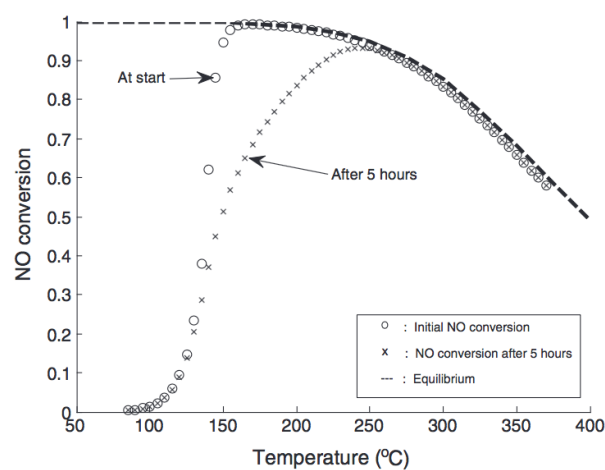


Fig. 12. Comparison of initial NO conversion and the conversion after exposing the catalyst to reaction conditions for 5 h (inlet NO = 450 ppm, O₂ = 6% and balance N₂).

results for the comparison of initial NO conversion and that obtained after exposing the catalyst to the reaction mixture for 5 h are shown in Fig. 12. It is observed that for intermediate temperatures (>130 °C and <250 °C), there is a difference between the initial NO conversion and that obtained after exposing the catalyst to the reaction conditions. However, at low and high temperatures, the curves essentially overlap indicating that the steady state activity of the catalyst is the same as initial activity. This is observed because of the low deactivation rates at low temperatures and the high rates of NO oxidation reaction at high temperatures, due to which the deactivated catalyst does not impact the NO conversion.

5. Conclusions

In this work, a global kinetic model is developed using a microkinetic approach to explain the reversible deactivation of a Pt/Al₂O₃ catalyst during NO oxidation. It is shown that the rates of deactivation and reactivation of the catalyst are dependent on the concentrations and temperature and the dominance of one over the other under specific conditions is responsible for the inverse hysteresis. The model considers the reversible deactivation of the catalyst due to both NO₂ and O₂ and the reactivation caused by the reduction of Pt oxides by NO. The highly oxidizing nature of NO₂ in comparison to O₂ is reflected in the kinetic constants used in the present model. The results of the proposed model are consistent with the experimental data reported in literature for various conditions. The model accurately predicts the effect of NO concentration, temperature ramp rate, and gas hourly space velocity on the light-off temperatures. It is shown that the kinetics of deactivation and reactivation are strongly dependent on the temperature, with the reactivation taking place at low temperatures (<140 °C) mainly in the presence of NO, and at high temperatures (>300 °C) by the decomposition of Pt oxides. The model predicts low values of the fraction of inactive Pt sites at moderate temperatures (~ 250 °C) during the temperature ramp-up in comparison to the case in which the same temperature is reached during the temperature ramp-down. This is explained by the kinetic limitations at lower temperatures, whereas near equilibrium conditions are achieved at high temperatures, resulting in high concentrations of inactive Pt sites. It is also shown that an increase in temperature beyond a particular temperature does not affect the trends in the inverse hysteresis behavior. Cooling down from a high temperature in the presence of N₂ alone is shown to result in getting activity

levels similar to the first temperature ramp, and is explained by the shift of equilibrium towards enhanced decomposition of Pt oxides. The effect of holding the temperature for a finite duration under various gas compositions is predicted to be consistent with the trends reported in the literature. In agreement with reported data, it is shown that exposing the catalyst to NO at low temperatures in the absence of O₂ for long time periods results in a high degree of catalyst reactivation.

The model predicts that for a fixed temperature, the time required for NO/O₂ system to achieve steady state is of the order of a few minutes for high and low temperatures, whereas it is of the order of a few hours for intermediate temperatures. These trends for the dependence of reaction temperature on the time taken to achieve steady state are consistent with the data reported on Pt/Al₂O₃ catalysts [7]. The results obtained in this study could be used to devise strategies for maintaining a high activity of a diesel oxidation catalyst.

Acknowledgements

The authors would like to acknowledge the support of Science and Engineering Research Board, Department of Science and Technology (Project No. SB/S3/CE/071/2014).

Appendix A. Supplementary material

Supplementary data associated with this article can be found, in the online version, at <http://dx.doi.org/10.1016/j.cej.2016.12.042>.

References

- [1] R. Marques, P. Darcy, P. Da, H. Mellott, Kinetics and mechanism of steady-state catalytic NO + O₂ reactions on Pt/SiO₂ and Pt/CeZrO₂, *J. Mol. Catal. A Chem.* 221 (2004) 127–136, <http://dx.doi.org/10.1016/j.molcata.2004.06.023>.
- [2] L. Olsson, H. Persson, E. Fridell, M. Skoglundh, B. Andersson, A kinetic study of NO oxidation and NO_x storage on Pt/Al₂O₃ and Pt/BaO/Al₂O₃, *J. Phys. Chem. B* 105 (2001) 6895–6906.
- [3] S.S. Mulla, N. Chen, W.N. Delgass, W.S. Epling, F.H. Ribeiro, NO₂ inhibits the catalytic reaction of NO and O₂ over Pt, *Catal. Lett.* 100 (2005) 267–270, <http://dx.doi.org/10.1007/s10562-004-3466-1>.
- [4] S.S. Mulla, N. Chen, L. Cumaranatunge, G.E. Blau, D.Y. Zemlyanov, W.N. Delgass, W.S. Epling, F.H. Ribeiro, Reaction of NO and O₂ to NO₂ on Pt: kinetics and catalyst deactivation, *J. Catal.* 241 (2006) 389–399, <http://dx.doi.org/10.1016/j.jcat.2006.05.016>.
- [5] J. Després, M. Elsener, M. Koebel, O. Kröcher, B. Schnyder, A. Wokaun, Catalytic oxidation of nitrogen monoxide over Pt/SiO₂, *Appl. Catal. B* 50 (2004) 73–82, <http://dx.doi.org/10.1016/j.apcatb.2003.12.020>.
- [6] D. Bhatia, *Kinetic and Modeling Studies of Catalytic Monolith Reactors and Lean NO_x Traps*, University of Houston, 2009.
- [7] D. Bhatia, R.W. McCabe, M.P. Harold, V. Balakotaiah, Experimental and kinetic study of NO oxidation on model Pt catalysts, *J. Catal.* 266 (2009) 106–119, <http://dx.doi.org/10.1016/j.jcat.2009.05.020>.
- [8] L. Olsson, E. Fridell, The influence of Pt oxide formation and Pt dispersion on the reactions NO₂ ↔ NO+1/2 O₂ over Pt/Al₂O₃ and Pt/BaO/Al₂O₃, *J. Catal.* 210 (2002) 340–353, <http://dx.doi.org/10.1006/jcat.2002.3698>.
- [9] W. Hauptmann, M. Votsmeier, J. Gieshoff, A. Drochner, H. Vogel, Inverse hysteresis during the NO oxidation on Pt under lean conditions, *Appl. Catal. B: Environ.* 93 (2009) 22–29, <http://dx.doi.org/10.1016/j.apcatb.2009.09.008>.
- [10] J. Li, A. Kumar, K. Kamasamudram, N. Currier, A. Yezerski, Time-dependent hysteresis in the NO oxidation to NO₂ on Pt-based catalysts, *Catal. Today* 258 (2015) 169–174, <http://dx.doi.org/10.1016/j.cattod.2015.04.035>.
- [11] C.P. Hwang, C.T. Yeh, Platinum-oxide species formed by oxidation of platinum crystallites supported on alumina, *J. Mol. Catal. A Chem.* 112 (1996) 295–302, [http://dx.doi.org/10.1016/1381-1169\(96\)00127-6](http://dx.doi.org/10.1016/1381-1169(96)00127-6).
- [12] M. Peuckert, H.P. Bonzel, XPS characterization of platinum oxides, *Surf. Sci.* 145 (1984) 239–259.
- [13] K. Hauff, U. Tuttles, G. Eigenberger, U. Nieken, Platinum oxide formation and reduction during NO oxidation on a diesel oxidation catalyst – experimental results, *Appl. Catal. B: Environ.* 123 (2012) 107–116, <http://dx.doi.org/10.1016/j.apcatb.2012.04.008>.
- [14] R.W. McCabe, C. Wong, H.S. Woo, The passivating oxidation of platinum, *J. Catal.* 114 (2) (1988) 354–367.
- [15] K. Hauff, H. Dubbe, U. Tuttles, G. Eigenberger, U. Nieken, Platinum oxide formation and reduction during NO oxidation on a diesel oxidation catalyst – macrokinetic simulation, *Appl. Catal. B: Environ.* 129 (2012) 273–281, <http://dx.doi.org/10.1016/j.apcatb.2012.09.022>.
- [16] D. Bhatia, R.D. Clayton, M.P. Harold, V. Balakotaiah, A global kinetic model for NO_x storage and reduction on Pt/BaO/Al₂O₃ monolithic catalysts, *Catal. Today* 147S (2009) S250–S256, <http://dx.doi.org/10.1016/j.cattod.2009.07.024>.
- [17] C.-B. Wang, C.-T. Yeh, Effects of particle size on the progressive oxidation of nanometer platinum by dioxygen, *J. Catal.* 178 (1998) 450–456, <http://dx.doi.org/10.1006/jcat.1998.2121>.
- [18] A.B. Mhadeshwar, H. Wang, D.G. Vlachos, Thermodynamic consistency in microkinetic development of surface reaction mechanisms, *ACS Div. Fuel Chem.* 48 (2013) 514–515.
- [19] <https://webbook.nist.gov>.
- [20] N. Seriani, W. Pompe, L.C. Ciacci, Catalytic oxidation activity of Pt₃O₄ surfaces and thin films, *J. Phys. Chem.* 110 (2006) 14860–14869.

